Hindawi
International Journal of Photoenergy
Volume 2017, Article ID 8547437, 19 pages
https://doi.org/10.1155/2017/8547437

Research Article

Mapping and Estimation of Monthly Global Solar Irradiation in Different Zones in Souss-Massa Area, Morocco, Using Artificial Neural Networks

O. Nait Mensour, S. Bouaddi, B. Abnay, B. Hlimi, and A. Ihlal

Materials and Renewable Energies Laboratory, Faculty of Sciences, Ibn Zohr University, BP 8106, Hay Dakhla, 80000 Agadir, Morocco

Correspondence should be addressed to O. Nait Mensour; omar.naitmensour@edu.uiz.ac.ma

Received 1 March 2017; Accepted 10 July 2017; Published 12 October 2017

Academic Editor: Philippe Poggi

Solar radiation data play an important role in solar energy research. However, in regions where the meteorological stations providing these data are unavailable, strong mapping and estimation models are needed. For this reason, we have developed a model based on artificial neural network (ANN) with a multilayer perceptron (MLP) technique to estimate the monthly average global solar irradiation of the Souss-Massa area (located in the southwest of Morocco). In this study, we have used a large database provided by NASA geosatellite database during the period from 1996 to 2005. After testing several models, we concluded that the best model has 25 nodes in the hidden layer and results in a minimum root mean square error (RMSE) equal to 0.234. Furthermore, almost a perfect correlation coefficient $R = 0.988$ was found between measured and estimated values. This developed model was used to map the monthly solar energy potential of the Souss-Massa area during a year as estimated by the ANN and designed with the Kriging interpolation technique. By comparing the annual average solar irradiation between three selected sites in Souss-Massa, as estimated by our model, and six European locations where large solar PV plants are deployed, it is apparent that the Souss-Massa area is blessed with higher solar potential.

1. Introduction

The solar radiation is the most abundant source of energy, with the earth receiving a heat flow ranging from 1.2 to 1.4 kW/m^2 [1], and it is a key factor impacting climate change [2, 3]. The growing concern and interest in energy conservation and environmental protection are driving the world towards a new era characterized by the energetic transition from almost total dependence on the fossil fuels to greater use of alternative renewable sources of energy [4]. Energy is indispensable to the economic and social development of humankind and is essential to ameliorate the quality of life. Morocco is the only North African country with no natural oil resources, about 93% to 97% of the energy demand is provided by imports [5, 6]. Morocco opted for changing its energy policy by adopting a green energy strategy focused on solar energy technologies especially in the country's southern areas [7] blessed with up to 3000 hours of the sunshine per year, which is equivalent to more than 6.5 kWh/m^2/day of irradiation [7]. To meet its energy needs, the solar energy represents a promising and abundant source of clean energy, which is expected to strongly contribute to the country's energetic mix. For a better energy collection and a higher efficiency of the solar collectors, the conception of many solar conversion systems, either solar or photovoltaic cells, requires the knowledge of solar radiation availability on horizontal and inclined planes [8–10]. Also, mapping solar radiation of an area is indispensable to evaluate the spatial variability of solar radiation and to examine the solar energy potential, which is important for engineers and researchers using solar energy systems [11]. Several relationships have been studied between solar radiation and several variables (e.g., temperature, precipitation, humidity, sunshine duration, cloud cover, elevation, latitude, and longitude) [12]. Currently, the models used for

the estimation of solar irradiation are based on statistical approaches which include conventional models such as regression methods, extrapolation, and time series, in addition to many methods based on artificial intelligence. It is worth noting that some of these models present serious limitations when it comes to nonlinear problems [13]. On the other hand, neural networks are considered to be the most advanced technique for solving these nonlinear problems by providing further precision and better estimation [14, 15]. Also, ANN modeling techniques provide a better solution for the estimation of solar radiation compared to other mathematical models, for instance, multiple regression [16], and present a high efficiency and rapidity of calculations. ANNs have widely accepted modeling and estimating tools used for providing an alternative way to solve complex and undefined problems [17], where the relationships between the variables of the system are difficult to represent by simple mathematical formulas.

Many individual studies have been performed for modeling solar irradiation in various locations (e.g., Spain [18], Thailand [19], Turkey [20], Malaysia [21], Italy [22], Nigeria [23], and China [24]). A study performed by Ouammi et al. estimated the global solar irradiation in different regions in Morocco [25]. This study showed that the Souss-Massa area is considered among the sunniest regions throughout the year.

In this study, we have developed ANN models that can be used to estimate global solar irradiation for any given location in the Souss-Massa area. These models were obtained by using geographical and meteorological data as input to the ANNs. This study area is near Ouarzazate City (see Figure 1) where the largest solar complex, one of the largest CSP plants in the world, is being built [26].

The aim of this study is twofold. The first is to develop feed-forward, back-propagation, multilayer perceptron (MLP) neural networks to estimate the monthly average daily global solar irradiation on horizontal surfaces. This was achieved by using the data of 175 locations distributed over the Souss-Massa area for 10 years (1996–2005). The best model selected used seven meteorological and geographical parameters as inputs for the ANN model (e.g., latitude, longitude, elevation, month of the year, sunshine duration, relative humidity, and mean temperature). The second is to explore the adequacy and reliability of using ANN models under different climatic conditions (desert, mountain, and coastal conditions) in the Souss-Massa area, as well as to investigate the ability of this technique to provide accurate results when modeling the nonlinear relationship between solar radiation and the geographical and meteorological parameters. The model developed is able to estimate the monthly mean solar irradiation for any given locations in Souss-Massa, where solar irradiation measurements are unavailable. The values of solar irradiation estimated by using the ANNs were presented in the form of monthly maps.

This paper is organized as follows: Materials and Methods describes the study area and introduces the data used in this research. Also, the ANN applied models are presented. The procedure used to select the model, the neural network architecture, and the selection inputs are explained in details in the same section. Results and Discussion explains the network optimization used in this study and presents the results of the estimations which are presented as monthly maps for the period from January to December. Also, a comparison between the selected towns showing different solar irradiation values is performed. Finally, conclusions are given on the ability of the model to give accurate estimations under different climatic conditions and across the different months in the studied area. The last paragraph is devoted to the comparison between the annual average solar irradiation of three selected sites in Souss-Massa, as estimated by our model, and six European locations where large solar PV plants are deployed.

2. Materials and Methods

This section introduces the study area, the data used for developing the model, and the general framework of ANN models. Also, the methodology followed for selecting, training, and testing the optimal model is explained.

2.1. Description of the Study Area. The Souss-Massa area, which is one of the twelve regions of Morocco, is located in the geographic coordinates 28°–31°N and 6°–10°W (Figure 1). This area is bordered to the west by the Atlantic Ocean, to the north by the Marrakech-Safi region, to the east by the Draa-Tafilalet area, to the southeast by Algeria, and to the southwest by the region of Guelmim-Oued Noun. The Souss River runs across the northern part of the region, which is in the valley between the Anti-Atlas and the High Atlas. Its capital is Agadir, which is located at the mouth of the Souss River [27]. The climate of the region is generally dry. It is influenced by both the Ocean and the Sahara. Regarding the precipitations, they are irregular in space and in time. The prevailing winds are either coming from the east or from the west. East and west winds are impacted by the desert and the freshness of the Ocean, respectively [28].

2.2. Description of ANN Models. Artificial neural network is a branch of artificial intelligence family (AI), which belongs to the group of computational algorithms called connectionist models [29]. ANN models were inspired by the functioning of real biological neurons such as the brain's behavior while processing information [30]. ANNs generalize the mathematical models of neural biology and the human cognition [31]. These models are known for their capability to learn from experience by making generalizations based on the previously seen information. A black-box representation of the system enables these models to perform a nonlinear mapping between multidimensional input space and multidimensional output space without any knowledge of the relationship between the input and output space [32]. This modeling tool is considered to be efficient and consumes less time during the modeling of complex systems compared to other mathematical models such as regression methods [17, 33]. Moreover, ANNs have been designed and developed by many researches from several

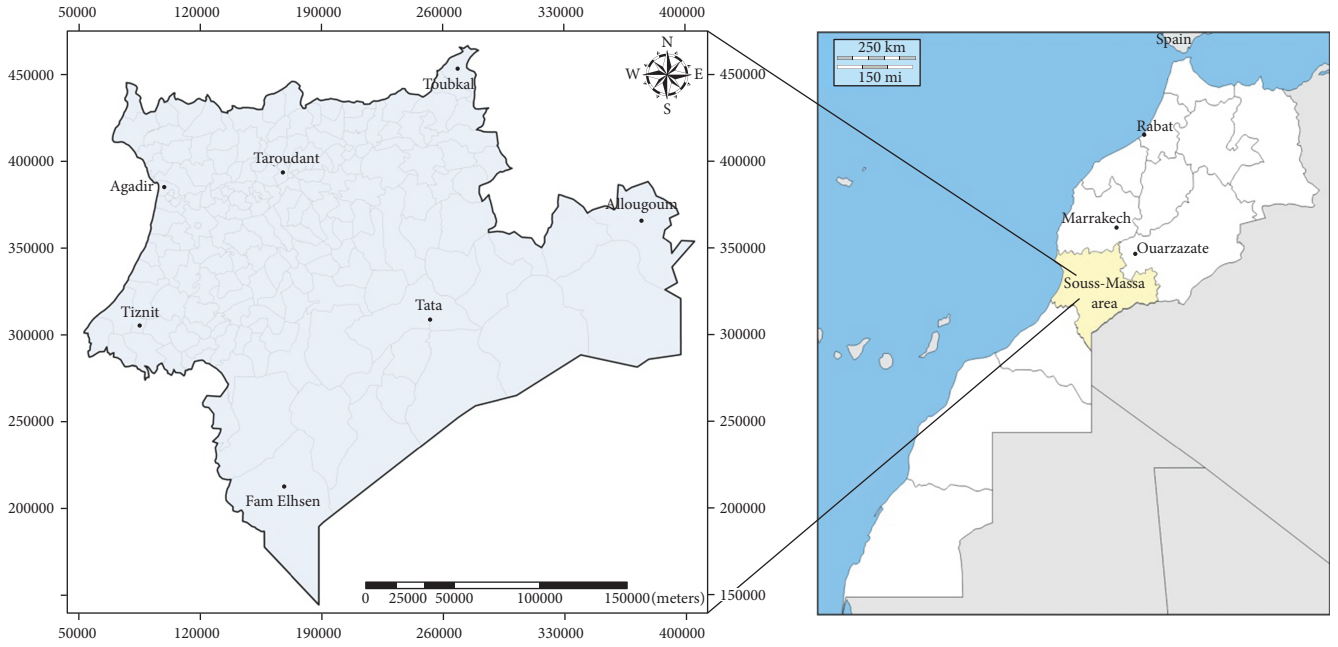

Figure 1: The Souss-Massa area study region.

scientific fields in order to solve the complex problem facing various disciplines such as pattern recognition, optimization, classification, prediction, vision, identification, and control systems [34]. The use of ANNs in recent years was extended to many complex engineering problems. The basic idea of neural networks is to utilize a single unit, a neuron, which is able to perform some basic calculations and then to connect a number of these units in the form of a network capable of solving more complex problems. The type and complexity of the application needed determine the structure of ANNs, the network size, and the learning mechanism employed. The neurons, also called nodes, form multiple connections and include generally five basic elements: inputs, weights and biases, a transfer function, a summing junction, and outputs. The neurons are organized in several layers formed by inputs, hidden layers, and an output layer.

The interconnection weights are important parameters of these models (see Figure 2). They are the components that are responsible for building the solving model based on the information provided to the network. The fundamental learning principle of this technique is to find a suitable algorithm to parameterize all the weights according to a specific goal to be fulfilled [35]. Once the adjustment of the weights is performed through different algorithms, the network weights are updated iteratively until the network provides the target outputs based on a given set of inputs. The network can be trained by supervised learning (i.e., when the inputs and the desired targets are exposed to the network) or unsupervised learning (i.e., when the network is left free without expected targets). The supervised training rule used by the back-propagation (BP) technique which consists back-propagating to the outputs

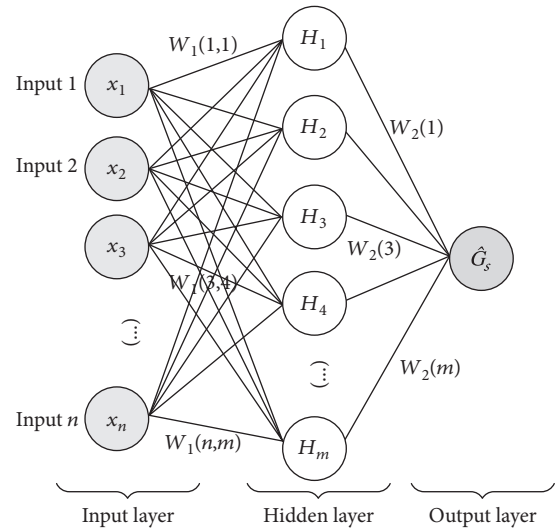

Figure 2: MLP, feed-forward neural network.

through the ANN and updating the weights until the mean square error (MSE), which is the difference between network's targets and outputs, becomes minimal [36, 37].

2.3. Description of the Used Data. The studied region has 175 sites (towns) in total. In our work, we operated by first designing the ANN best model by using a selection of 24 site representatives of the different climates of the region in order to obtain a robust design. Then, the designed ANN is used in estimating the solar irradiation in the remaining 151 sites.

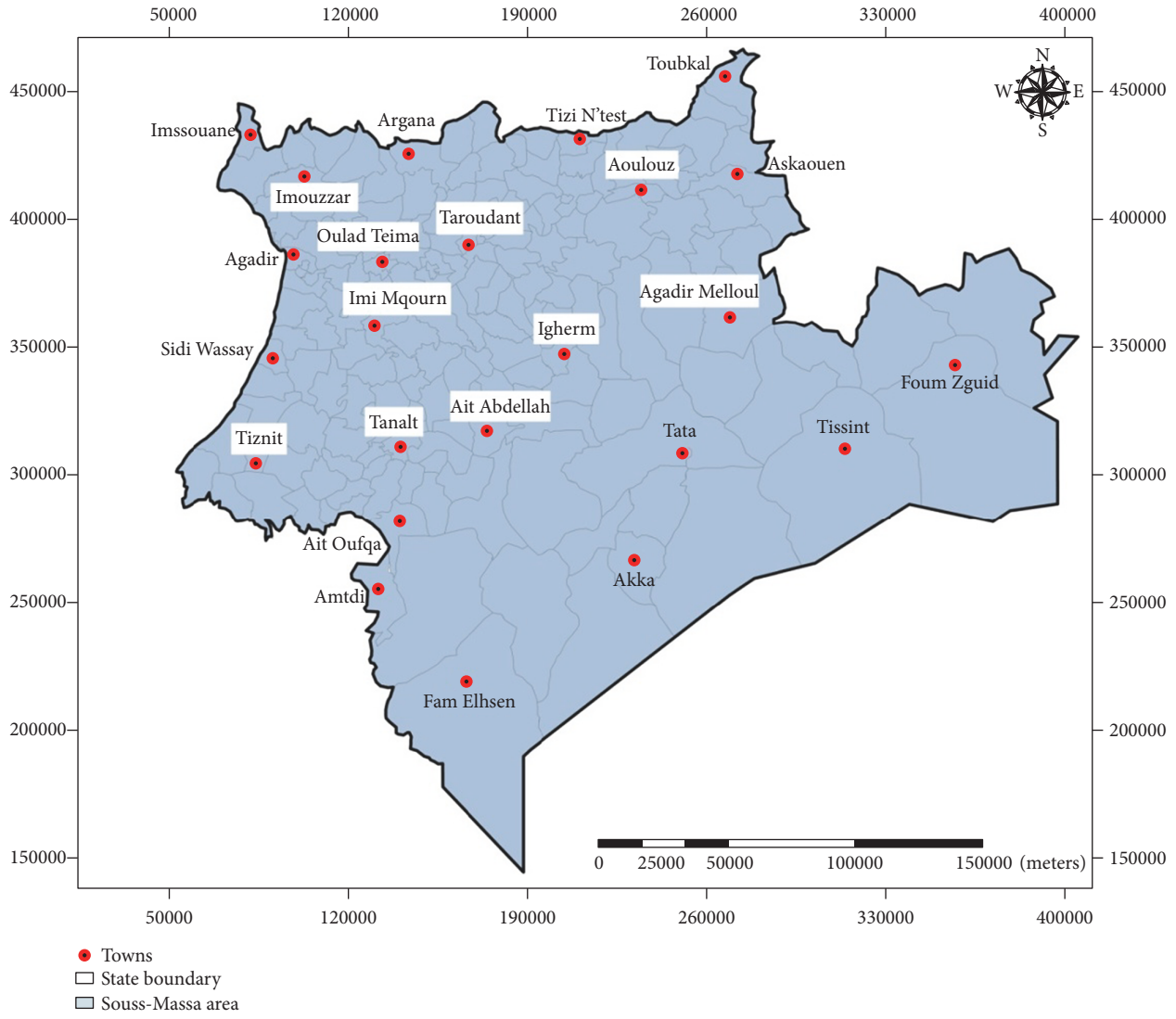

Figure 3: The selected towns used to train and test the ANNs.

The geographical and meteorological data of 175 sites used in this study were obtained from Google Maps such as latitude, longitude, and elevation, and the average monthly meteorological parameters (mean temperature, mean sunshine duration, mean relative humidity, and solar irradiation) were taken from NASA geosatellite database for 10 years (1996–2005). Also, the monthly periods of the year are included in the analysis. According to methodology given by NASA [38], the solar irradiation and other meteorological data estimated by satellite are compared and calibrated with the ground stations located around the world [39]. Moreover, solar radiation is compared with data from the Baseline Surface Radiation Network (BSRN) [40]; thus, they can be considered as measurements. Furthermore, there are many studies that used these solar irradiation data as measurement values [15, 23, 41]. These data were used in our study because they are the only publicly available data covering a long period in the studied region. Therefore, eight geographical and meteorological parameters identified above were involved in this study. In the designing of the ANN models, we have used the data of 24 sites in the Souss-Massa area for training and testing our models developed; see Figure 3. For each of these 24 locations, we have collected eight parameters which include, as mentioned earlier, the solar irradiation that we want to estimate. In the following sections, we will represent in details the procedures followed to design, select, train, and test the models.

2.4. Design of ANN Models. ANN models are defined by their architecture, learning, or training algorithm and their activation function. In this study, we adopted ANNs following a multilayer perceptron (MLP) feed forward back-propagation (BP). Different architectures were constructed using the Matlab Neural Networks Toolbox version 8.1.0 [42]. The designed networks are comprised of three layers: the input layer, hidden layer, and the output layer; connection weights and biases; activation function; and summation node (a visual scheme is shown in Figure 2). The choice of appropriate sets of input parameters is essential in ANN

Table 1: Error values and the correlation coefficient of different ANN configuration models.

Configurations	Number of neurons in hidden layer	MAE	RMSE/rRMSE	R
Lat, Long, Al, Mn	34	0.248	0.314 (5.46%)	0.974
Lat, Long, Al, Mn, Sh	34	0.249	0.312 (5.43%)	0.975
Lat, Long, Al, Mn, Sh, T	27	0.227	0.286 (4.97%)	0.979
Lat, Long, Al, Mn, Sh, H	33	0.204	0.262 (4.56%)	0.983
Lat, Long, Al, Mn, T	32	0.233	0.294 (5.11%)	0.978
Lat, Long, Al, Mn, H	34	0.217	0.274 (4.77%)	0.980
Lat, Long, Al, Mn, Sh, T, H	25	0.184	0.234 (4.07%)	0.988

modeling [43, 44]. If pertinent inputs are excluded, the model will not be able to identify accurately the desired input-output relationship. Generally, a set of candidate input parameters is found through a priori knowledge of the system to be modeled. Hence, the choice of inputs for the network was based on several criteria. For example, to account for the geographical location of the sites, the parameters of latitude and longitude are introduced. The use of the elevation parameter is selected to account for mountainous and flat zones. Concerning the choice of temperature and relative humidity, they are closely related to solar radiation [45, 46]. Finally, since our study aims at estimating monthly global solar irradiation, it is necessary to include the parameters of the month of the year and sunshine duration as inputs.

In order to design the best suitable configuration to our problem, that is, to select the appropriate set of input variables corresponding to a single output that we want to estimate, different configurations of the inputs are developed as shown in Table 1. To perform this selection, different networks with a single layer were used by combining the variables of latitude, longitude, elevation, month of the year, sunshine hours, mean temperature, and mean relative humidity. Moreover, the number of nodes in the hidden layer was varied from 1 to 40. Concerning the datasets input/target, they were randomly divided into three subsets: training, validation, and testing datasets. The training set represents seven-tenths (70%, i.e., 2016 data points) of the dataset used for updating network parameter weights and biases, whereas three-tenths (30%, i.e., 864 data points) of the entire dataset was used for validation and testing. Each configuration forming the network was tested 10 times by trying randomly various weights and biases. Then, the performance of each network with different configurations is assessed based on the root mean square error (RMSE) and the correlation coefficient (R value) between the estimated and measurement values; see Section 2.5.

The purpose of this procedure is to determine the network with the best ability to accurately estimate the solar irradiation intensity.

The used activation function ψ in the hidden layer is defined by the sigmoid function $\psi = 1/1 + e^{(-x)}$ with x being the corresponding input. Regarding the output layer, we have used a linear function φ as an activation function [47].

The final output function, $\widehat{G}_s$, which represents the monthly average global solar irradiation estimated, is defined as follows:

$$\widehat{G}_s(X) = \varphi\left(\sum_{i=1}^{H} H_i \cdot W_2(i) + b_2\right), \tag{1}$$

where

$$H_i(X) = \psi\left(\sum_{j=1}^{N} X_j \cdot W_1(i,j) + b_1(i)\right). \tag{2}$$

Here, X is the input parameter and H_i is the response of the ith hidden neuron. $W_1(i,j)$ and $W_2(i)$ are the weight between ith hidden layer neuron and jth input and the weight between the output neuron and ith hidden layer neuron, respectively.

Concerning the bias terms, $b_1(i)$ refers to the bias value applied to the ith hidden layer neuron, while b_2 refers to the bias value applied to the output layer neuron.

In order to ensure the best generalization capabilities to enhance the ANN models and avoid overfitting, we have used the early stopping method [37, 42], which is a method for stopping the training phase when overfitting starts during supervised training. This technique is automatically supplied for all supervised network creation function including the back-propagation network. Early stopping is generally used because it is easy to understand and implement and is considered to be, in many cases, better than regularization methods [48]. The data are divided into three subsets: the first subset is the training set, the second is the validation set, while the remaining subset is used for testing [49]. Levenberg-Marquardt (implemented as Trainlm in MATLAB software), which is a network training algorithm, is used in this work according to the Levenberg-Marquardt (LM) optimization technique [50, 51]. The LM supervised algorithm combines the positive features of Gauss-Newton algorithm (GN) and gradient descendent (GD) to build a hybrid optimization technique, which is adequate for many real applications. More interestingly, LM algorithm is known for its fast convergence [52].

2.5. Selection of the Optimal ANN Model. The selection of the model with the best performance is validated by using the following statistical scores [53]: MSE (mean square error), MAE

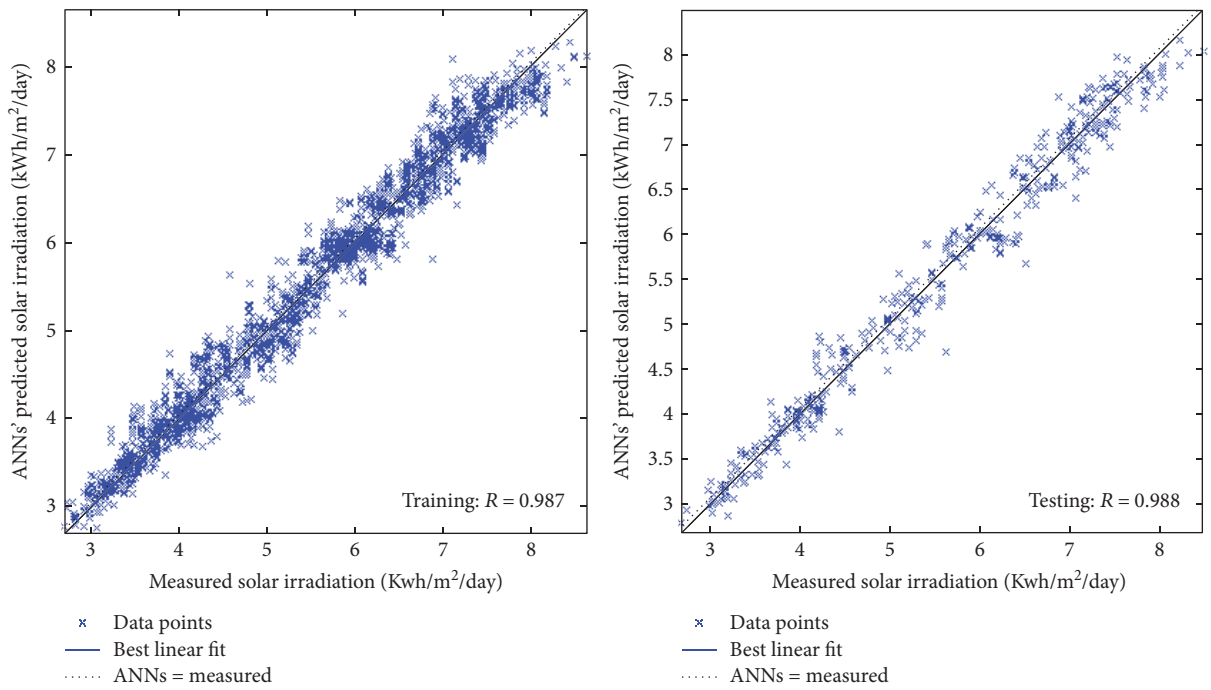

Figure 4: The scatter plot of ANN estimated solar irradiation measured data for training set and testing set.

(mean absolute error), RMSE (root mean square error), rRMSE (relative root mean square error), and the correlation coefficient (R) between estimated and measured values of monthly average daily global solar irradiation for both training and testing datasets. The formulas for these selection criterions are expressed as follows:

$$\begin{aligned}
\mathrm{MSE} &= \frac{1}{n}\sum_{s=1}^{n}\left(G_s - \widehat{G}_s\right)^2,\\
\mathrm{MAE} &= \frac{1}{n}\sum_{s=1}^{n}\left(G_s - \widehat{G}_s\right),\\
\mathrm{RMSE} &= \sqrt{\sum_{s=1}^{n}\frac{\left(G_s - \widehat{G}_s\right)^2}{n}},\\
\mathrm{rRMSE}\,(\mathrm{in}\%) &= \mathrm{RMSE}\times\frac{100}{\overline{G}},\\
R &= \frac{\sum_{s=1}^{n}\left(G_s - \overline{G}\right)\left(\widehat{G}_s - \overline{\widehat{G}}\right)}{\sqrt{\sum_{s=1}^{n}\left(G_s - \overline{G}\right)^2\sum_{s=1}^{n}\left(\widehat{G}_s - \overline{\widehat{G}}\right)^2}},
\end{aligned} \tag{3}$$

where $\widehat{G}_s$ is the estimated global solar irradiation and G_s is the measured global solar irradiation. $\overline{G}$ refers to the average measured global solar irradiation, while $\overline{\widehat{G}}$ is the average estimated global solar irradiation. Here, n is the number of input/output sample.

After testing several configurations, we selected the model with the minimum error between the actual and estimated values and with the best correlation coefficient.

Table 1 shows the different configurations tested in order to select the model with the optimum estimation capability. As we can observe from this table, the best model has seven ($N = 7$) input variables (latitude (Lat), longitude (Long), elevation (Al), month of the year (Mn), sunshine duration (Sh), mean temperature (T), and relative humidity (H)) and includes twenty-five nodes ($H = 25$) in its hidden layer. This configuration results in a 4.07% relative root mean square error. Figure 4 displays the correlation coefficient (R) of this model showing $R = 0.988$ for testing and $R = 0.987$ for training.

2.6. Training and Testing of the Model. The training phase is the most important step to build efficient ANNs. Hence, it is necessary to perform it carefully and wisely. Four stages are usually essential during the training process: the collection of the training data, the design of the network, the training of the network, and the simulation. After a sufficient training period, which can take a considerable capacity of the computer's memory and time, the trained network acquires the ability to figure out the nonlinear relationships between input and output parameters. Therefore, the model is able to easily estimate the output data when new input data, unseen by the network and not used in the training phase, are fed to the system. It is important to train various networks in order to make sure that the network is working with the maximum possible generalization capability. As mentioned earlier, each network will be trained by different initial weights and biases. Also, prior to the training phase, the network inputs and targets were normalized in the range [−1, 1].

In the previous section, we have shown the followed test procedure to select the most suitable model based on the minimum error. For further analysis, we added another test to the optimal network model, which is the set that contains 7 input variables and 25 nodes in the hidden layer. In the current work, two tests were used. The first test was randomly

Table 2: The geographical data of the locations selected to test the network under different climatic conditions.

Towns	Latitude (°N)	Longitude (°W)	Altitude (m)	Climate types
Aglou	29.804	9.834	2	Coastal
Biogra	30.220	9.372	130	Dry
Amskroud	30.529	9.331	280	Dry, semiarid
Tiout	30.384	8.697	460	Semiarid
Akka Ighan	29.992	7.532	788	Desert climate
Tafraoute	29.718	8.976	999	Mountain, dry
Tailouine	30.532	7.925	1027	Mountain
Issen	30.682	9.152	1138	Mountain

carried out by the ANN model using 15% of the data of the 24 locations. The second test, which is the manual test, uses the data which are neither seen by the network nor used in the training phase. In order to perform this manual test, that is, to make sure that the network developed is able to estimate monthly global solar irradiation in different prevailing climate in the area, we have randomly selected some locations of the region. Table 2 shows the geographical data of the locations selected to test the network before starting the step's estimation. The selected sites are characterized by different climates (mountainous, coastal, and desert zones) and are located in the north, south, east, and west. The input dataset for these eight selected locations is unseen by the network during the training phase. Figure 5 shows the geographical positions of the different locations used in the manual test.

After performing the tests on the ANN model developed by using inputs from different locations representing various climatic conditions, we estimated solar irradiation for the period 1996–2005. Then, we compared the obtained results with the actual values.

Figure 6 illustrates the variation of monthly average solar irradiation for ten years (1996–2005).

Figure 6 shows the difference between the measured and estimated monthly mean global solar irradiation in eight locations. By observing these differences, it is clear that our model is able to estimate solar irradiation for most of the test areas with a relatively good accuracy, except for some towns where we noticed a fairly low margin of errors between the measured and estimated values, especially for mountainous zones for instance: Tafraoute and Issen. The relative mean square error was estimated to be around 2.77% for the whole dataset used for testing.

3. Results and Discussion

This section presents the estimation of monthly solar irradiation based on the ANNs. Also, the obtained solar irradiation results of the Souss-Massa area are mapped.

3.1. ANN Estimations. According to the results reported in Table 1, where the optimization of the network is illustrated, the ANN with a single hidden layer and twenty-five nodes trained by the LM algorithm provides the best performance compared to other suggested networks. As stated before, the R values of 0.987 and 0.988 were obtained for training and testing datasets, respectively.

In order to select the best model, the testing session is performed by using the same 24 sites. These tests have been randomly performed by the network. In order to produce the monthly average solar irradiation maps of the Souss-Massa area with the maximum possible accuracy, the manual test with the dataset which is not used in the training was performed in different locations representing different climates of the region (Figure 5). To estimate the solar intensity, we used the geographic and meteorological parameters as input for the optimal ANN model, that is, the latitude, longitude, elevation, months of the year, mean temperature, mean sunshine duration, and relative humidity. By training ANN with 24 locations, we have estimated the solar potential of about 151 sites of the entire region. Finally, the estimated monthly average solar irradiation is presented using twelve maps, each one illustrating a month of the year, from January to December (see Figures 7–18). These maps were generated by using the geographical information system (GIS) software Arc Map with the integrated Kriging interpolation analysis. This interpolation technique estimates values for cells into a raster from a limited number of sampling points. It can be used to estimate unknown values for any geographic point data [54].

3.2. Monthly Solar Irradiation Maps in the Souss-Massa Area. Mapping solar energy potential is necessary for designing solar power systems and essential for selecting suitable sites for deploying solar technologies. Table 3 displays the maximum potential values of monthly mean daily global solar irradiation, as well as the minimum and standard deviation (std) values obtained in the Souss-Massa region. Here, the monthly mean daily solar irradiation varies between 2.04 kWh/m^2/day as a minimum and 7.92 kWh/m^2/day as a maximum, respectively, in December and May. Furthermore, this table confirms, as it is widely known by Moroccan stakeholders and decision makers, that the most interesting sites for deployment of solar power plants are the regions located in some inland regions and in the southern-eastern territories.

The solar maps of the studied region during an entire year were obtained using a color gradient from low to high intensity to show the energy potential in different locations.

Figures 7–10 display the solar irradiation maps of the Souss-Massa area during the months of November, December, January, and February, respectively, as estimated by the ANN technique. The solar irradiation value varies between 3.63 kWh/m^2/day and 4.17 kWh/m^2/day in November, 2.83 kWh/m^2/day and 3.52 kWh/m^2/day in December, 3.29 kWh/m^2/day and 4.04 kWh/m^2/day in January, and between 4.37 kWh/m^2/day and 5.02 kWh/m^2/day in February. These months show the lowest irradiation intensity throughout the year because the winter solstice has already started. The figures above exhibit a similar behavior. It can be seen that some inland areas including the center and south-eastern territories show a higher solar irradiation than other sites,

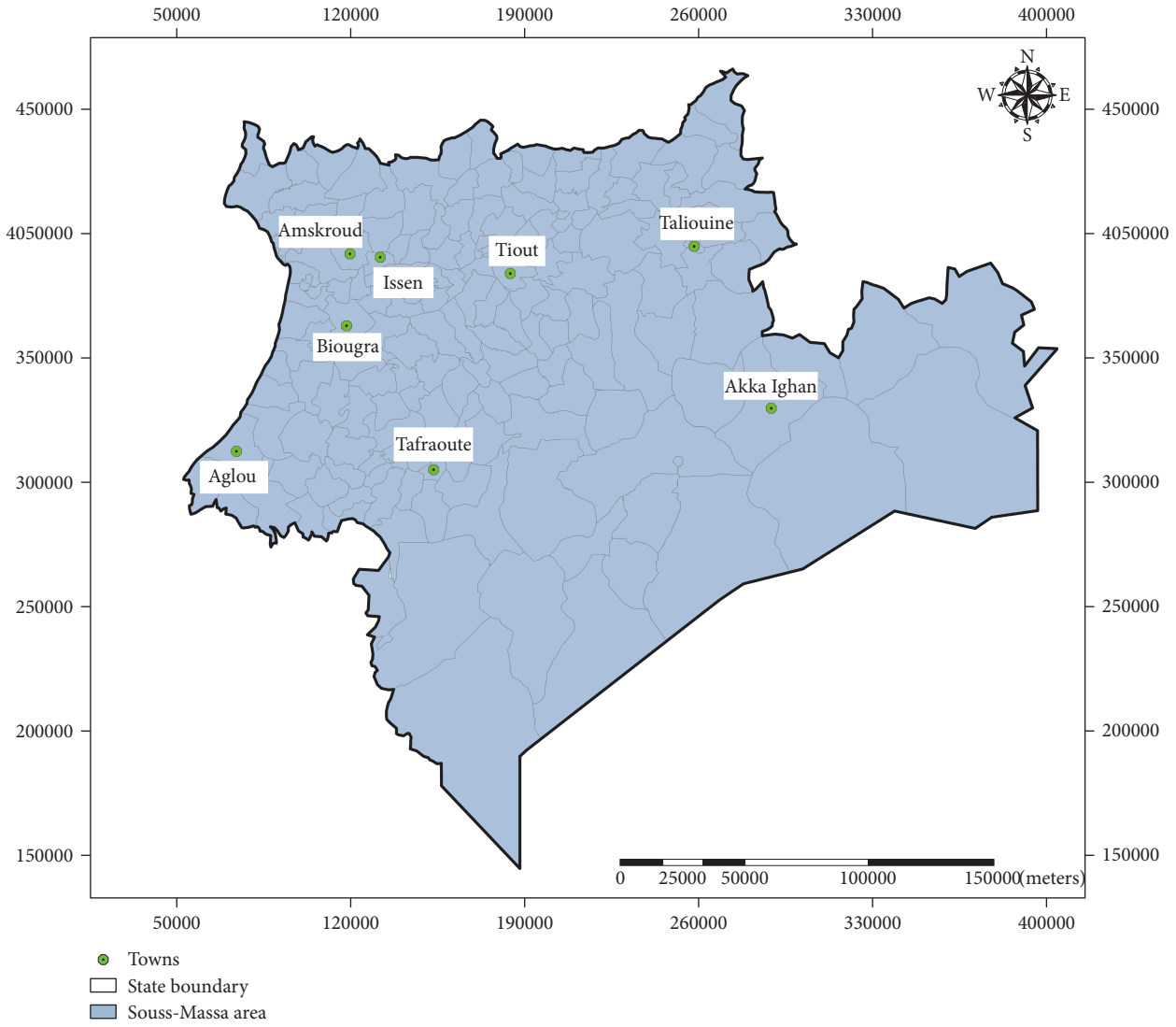

Figure 5: The geographical locations used in the test under different climatic conditions.

making them suitable locations for solar technologies requiring high solar irradiation. These locations can be advantageous to build an efficient peak power control during these months. Moreover, such a high irradiation is crucial to cover the energy demand supply.

Figures 11 and 12 illustrate the solar irradiation maps as obtained by the ANN method in March and April, respectively, in the Souss-Massa area. The estimated values of solar irradiation range between 5.28 and 6.08 kWh/m^2/day in March versus 5.83 and 7.19 kWh/m^2/day in April. The analysis of these figures shows that solar irradiation starts to increase in the Atlantic coasts, especially in Agadir territory and in the center of the region. The southern-eastern locations receive a substantial amount of solar potential whereas the locations enclosed by the Atlas Mountain and a portion of the Western Atlantic costs (Tiznit territory) always display a similar behavior, which consists of receiving a low amount of solar energy compared to the other locations.

Figures 13 and 14 show the solar irradiation maps obtained by using the ANN technique in the Souss-Massa area during May and June. Here, the highest solar intensity reached is between 7.92 and 7.87 kWh/m^2/day, while the lowest intensity is between 5.50 and 5.18 kWh/m^2/day in May and June, respectively. From May onwards, it can be seen from these figures that the solar potential reaches a maximum in Southeast and some other places. By observing the results obtained during June, we can notice that the mountains located in the Northern region receive a considerable amount of solar irradiation compared to other months of the year. As usual, the towns that are located on the Atlantic coast (west of the area) receive less solar irradiation relative to other locations in the area.

Figures 15 and 16 display solar potential maps obtained by the ANN technique in July and August, respectively. The solar potential starts to increase and reaches its maximum in the Atlas Mountains, as well as at some inland locations of the region. In this case, the same distribution of solar

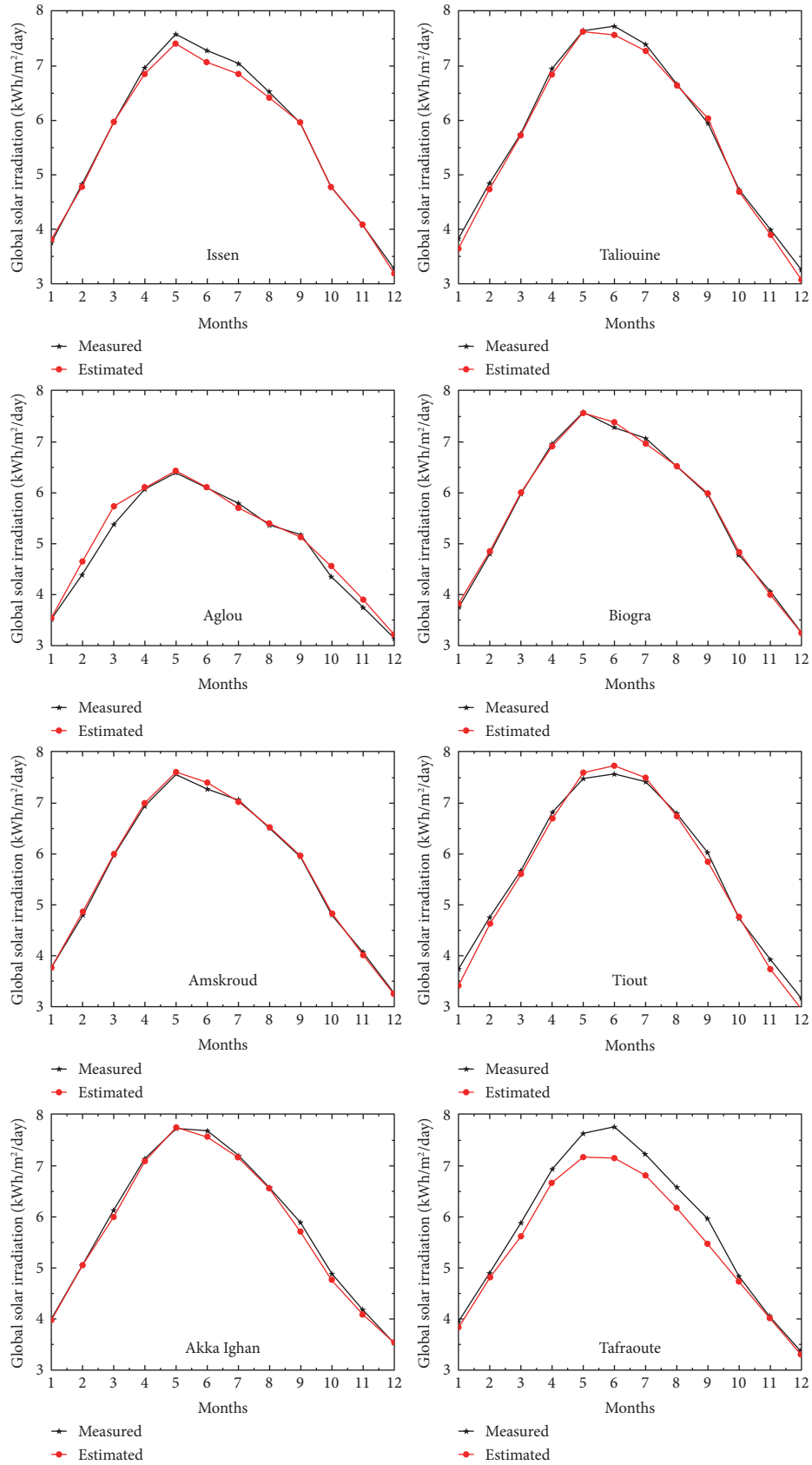

Figure 6: Comparison of the monthly mean global solar irradiation between measured and estimated values for eight locations used in the test under different climatic conditions during the period 1996–2005.

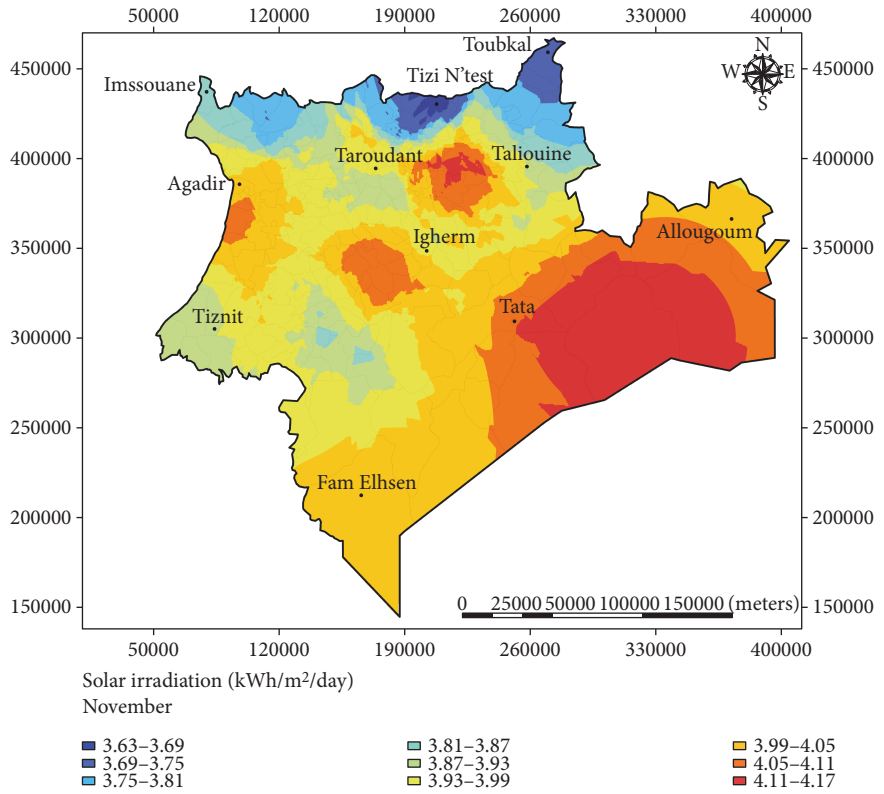

Figure 7: Solar energy potential map of the Souss-Massa area for the month of November as estimated by the ANN and designed with the Kriging interpolation technique.

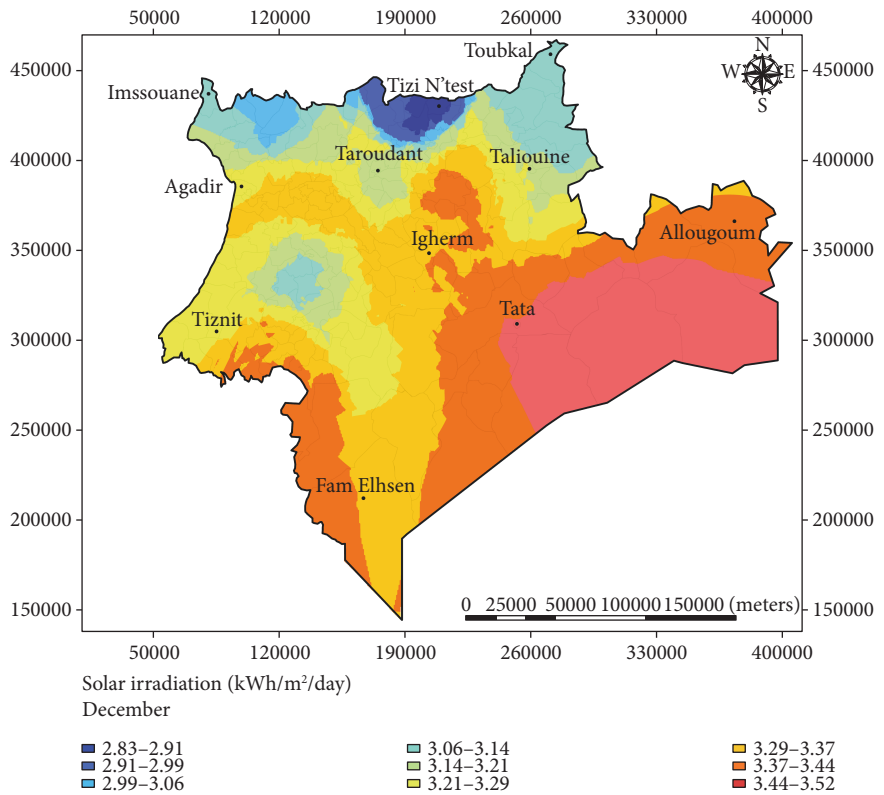

Figure 8: Solar energy potential map of the Souss-Massa area for the month of December as estimated by the ANN and designed with the Kriging interpolation technique.

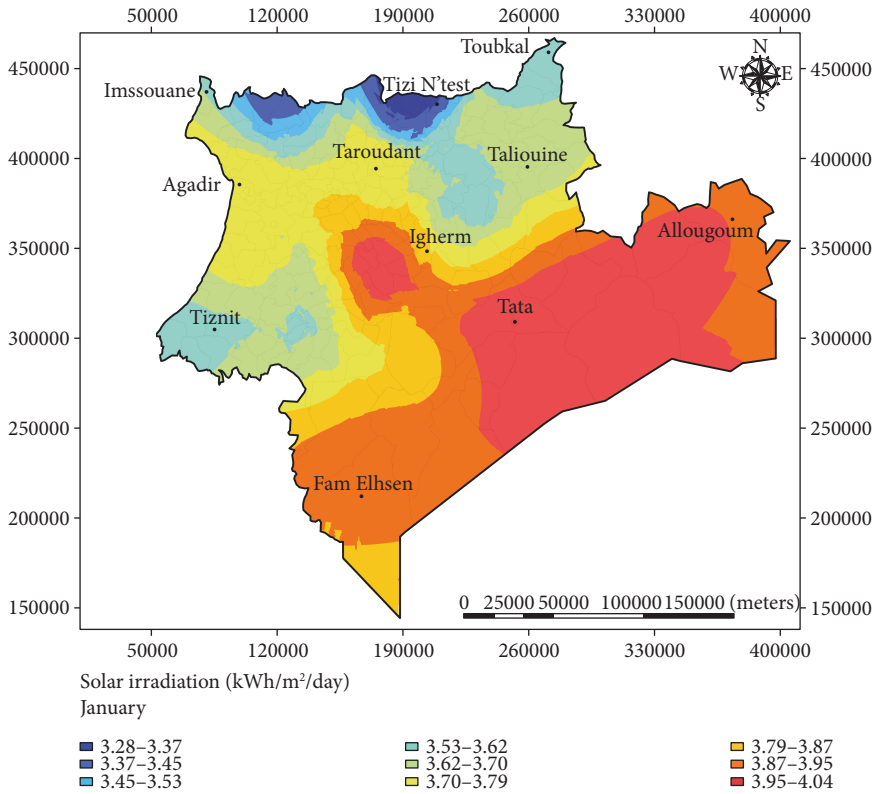

Figure 9: Solar energy potential map of the Souss-Massa area for the month of January as estimated by the ANN and designed with the Kriging interpolation technique.

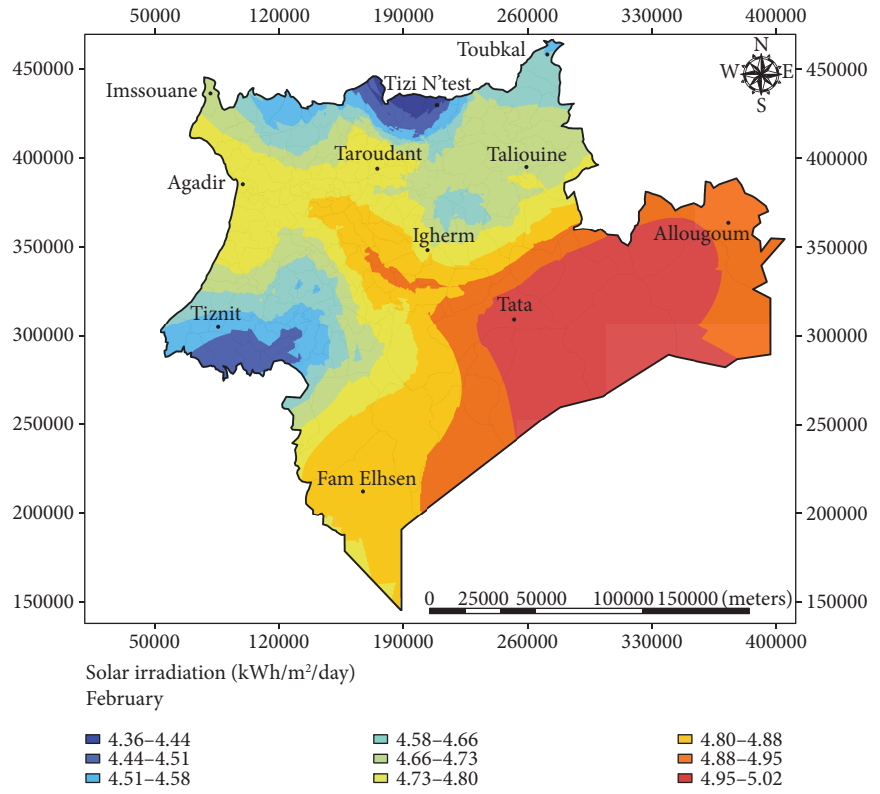

Figure 10: Solar energy potential map of the Souss-Massa area for the month of February as estimated by the ANN and designed with the Kriging interpolation technique.

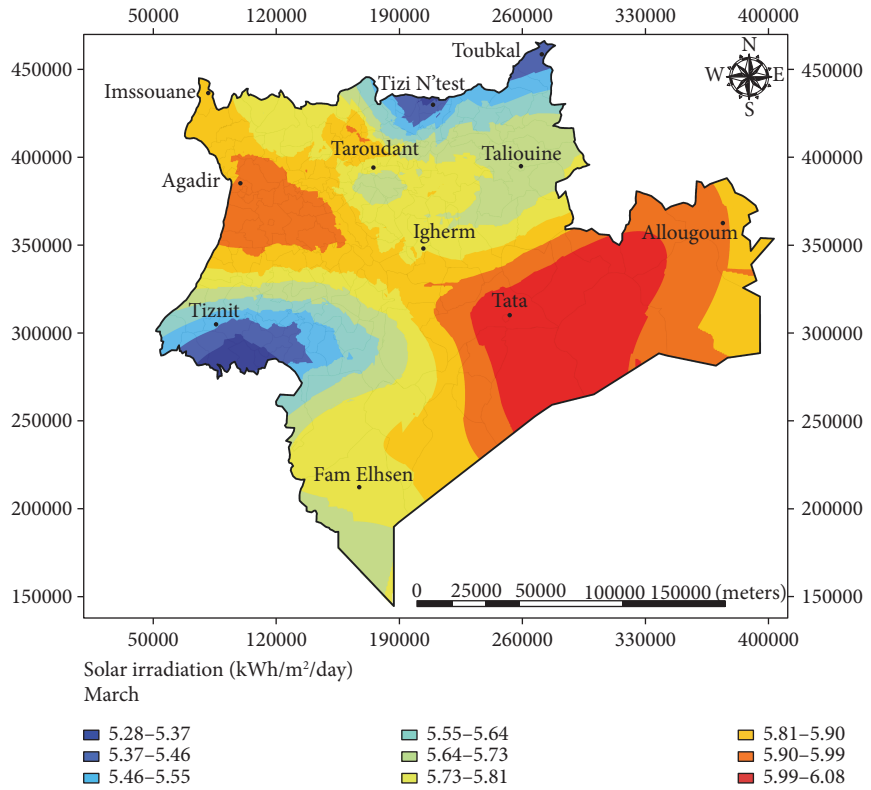

Figure 11: Solar energy potential map of the Souss-Massa area for the month of March as estimated by the ANN and designed with the Kriging interpolation technique.

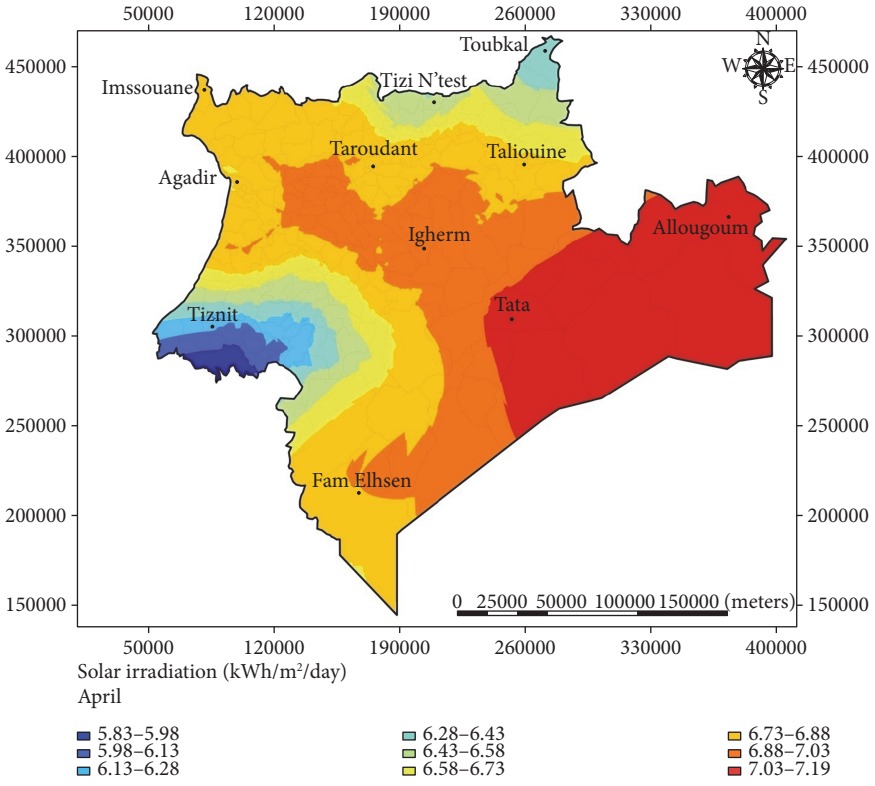

Figure 12: Solar energy potential map of the Souss-Massa area for the month of April as estimated by the ANN and designed with the Kriging interpolation technique.

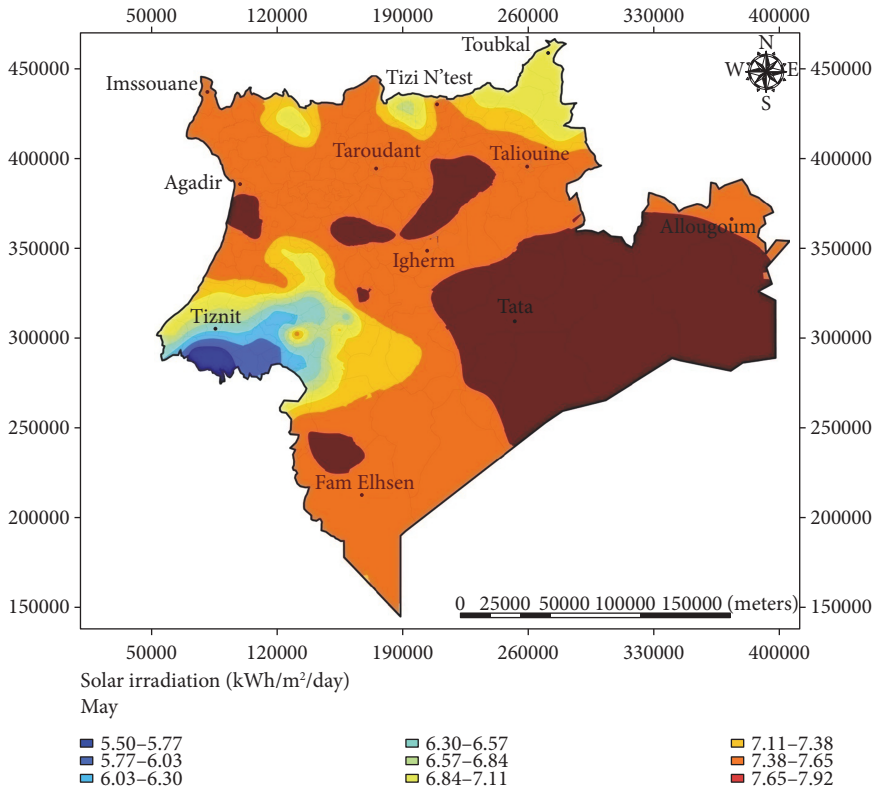

Figure 13: Solar energy potential map of the Souss-Massa area for the month of May as estimated by the ANN and designed with the Kriging interpolation technique.

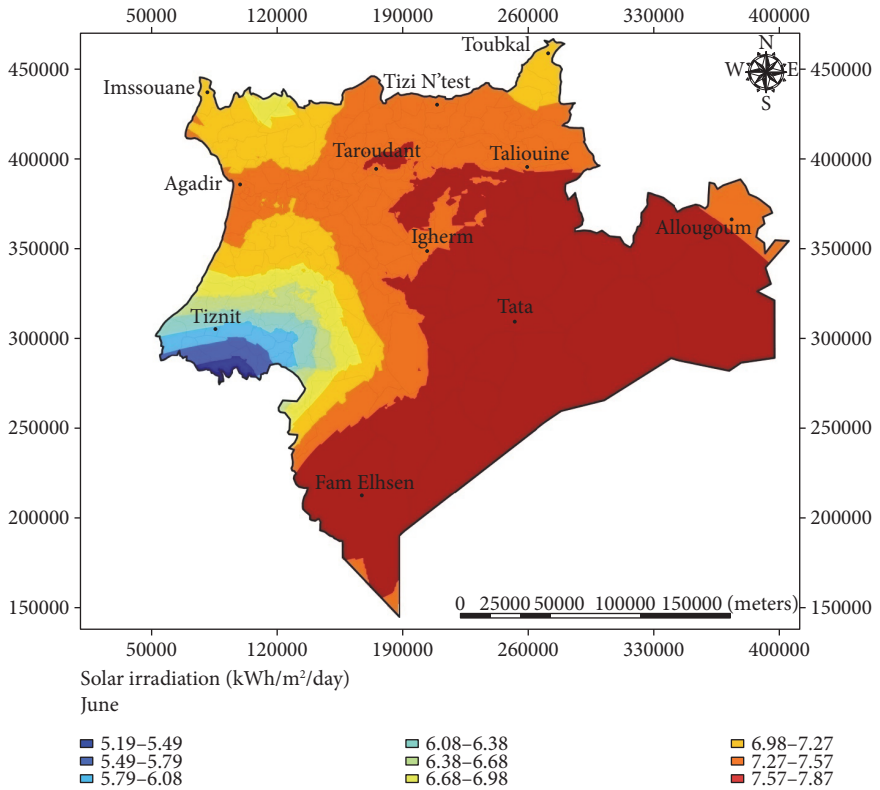

Figure 14: Solar energy potential map of the Souss-Massa area for the month of June as estimated by the ANN and designed with the Kriging interpolation technique.

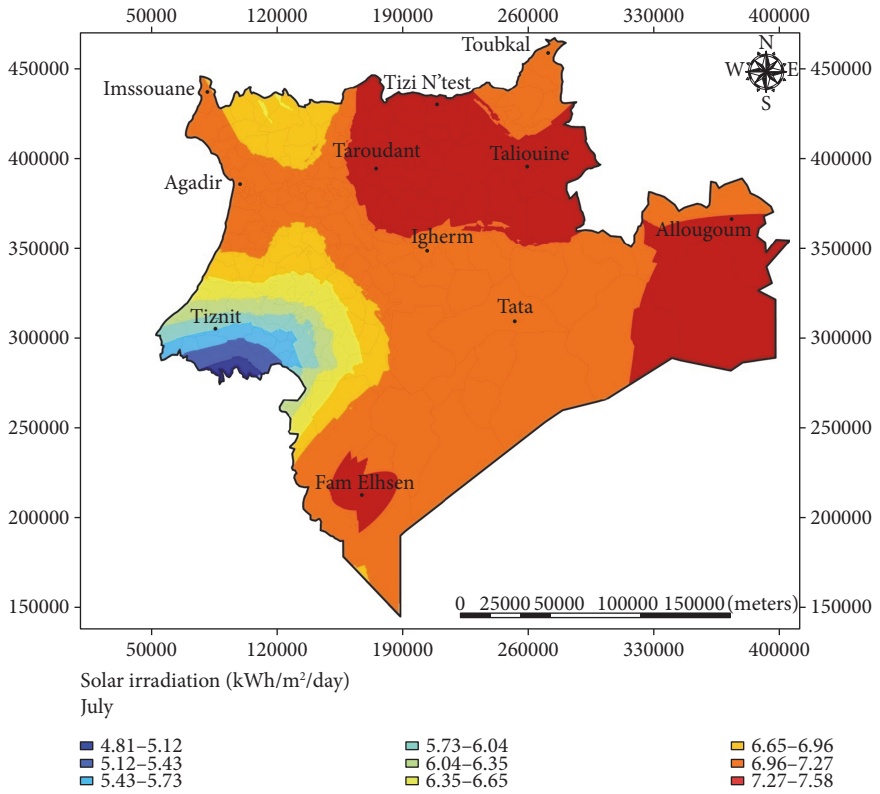

Figure 15: Solar energy potential map of the Souss-Massa area for the month of July as estimated by the ANN and designed with the Kriging interpolation technique.

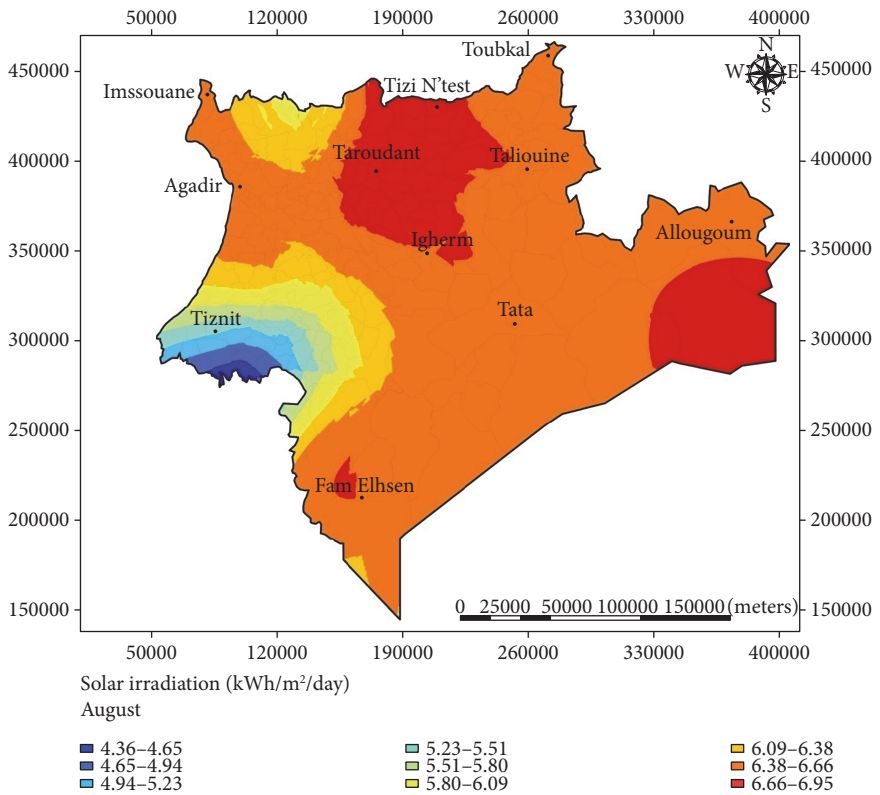

Figure 16: Solar energy potential map of the Souss-Massa area for the month of August as estimated by the ANN and designed with the Kriging interpolation technique.

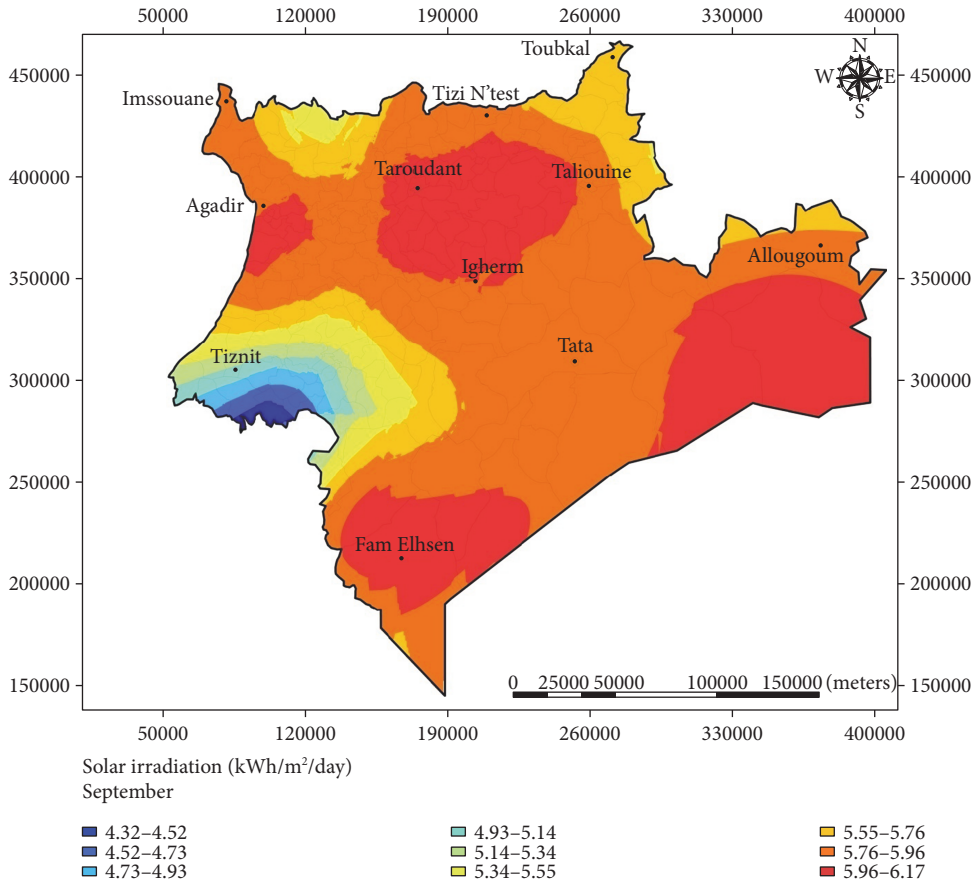

Figure 17: Solar energy potential map of the Souss-Massa area for the month of September as estimated by the ANN and designed with the Kriging interpolation technique.

potential for both July and August is obtained in most of the southern and eastern locations, in addition to some towns of the Atlantic coasts and the center of the area. For example, the estimated solar irradiation varies between 4.80 and 7.58 kWh/m^2/day in July versus 4.35 and 6.94 kWh/m^2/day in August.

Figures 17 and 18 show the solar irradiation maps of the Souss-Massa area during September and October. The estimated intensity of solar irradiation ranges between 4.32 and 6.15 kWh/m^2/day in September versus 4.38 and 5.04 kWh/m^2/day in October. Also, it is clear that the most promising locations during September are the inland locations especially in the center of the area, in addition to southern locations and some territories of the Atlantic coast such as Agadir. Concerning October, the solar irradiation intensity starts to decrease in most locations, especially in places enclosed by the Atlas Mountains and the Atlantic coast (Tiznit). The southeast region, on the other hand, receives the maximum solar potential. Thus, it is considered to be a promising location.

By using the estimations of the best ANN model found based on the methodology presented in this paper, the solar energy potential of various locations in the Souss-Massa area is obtained, which is considered to be valuable information for the deployment of solar energy plants.

3.3. Comparison of Solar Potential between the Souss-Massa Area and Other Zones in Europe. This section provides a simple comparison of the solar potential between the Souss-Massa area and some selected sites in Europe. These selected European sites present high solar potential and are considered to be among the largest photovoltaic power plants in the world [55]. Table 4 illustrates the locations of photovoltaic solar plants deployed in Germany and Spain and their corresponding nominal capacity.

To perform this comparison, we have collected the monthly average global solar irradiation data for each city where the stations are installed. The data of the six selected European stations are obtained from Photovoltaic Geographical Information System (PVGIS) [56] (see Table 5), while the data of three cities (Agadir, Tata, and Taroudant), which are among the sunniest locations in the Souss-Massa area during the entire year, are provided by our previous analysis.

According to the values presented in Table 5, the monthly average global solar irradiation intensity of the three sites located in Germany ranges between 0.55 kWh/m^2/day as minimum in December and 5.64 kWh/m^2/day as maximum in June. In Spain, the lowest intensity is around 1.89 kWh/m^2/day, while the highest is around 7.74 kWh/m^2/day in December and July, respectively.

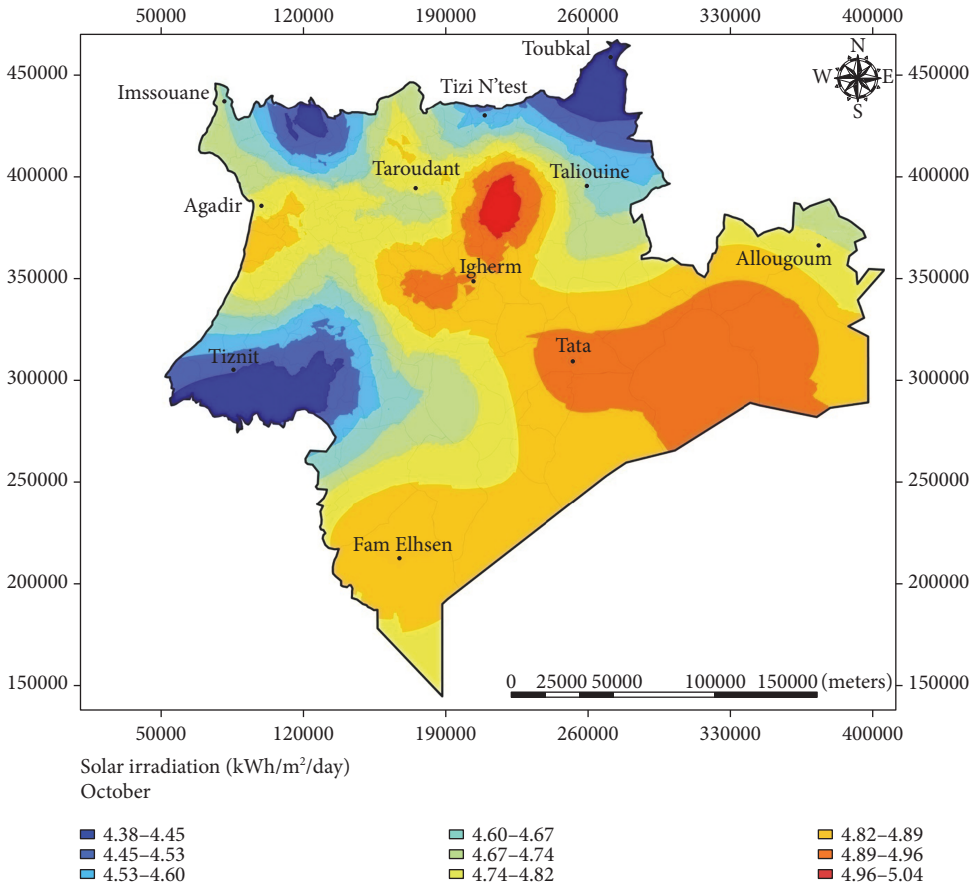

Figure 18: Solar energy potential map of the Souss-Massa area for the month of October as estimated by the ANN and designed with the Kriging interpolation technique.

Table 3: Mean, minimum, maximum, and standard deviation of monthly mean daily global solar irradiation in the Souss-Massa area.

Month	Solar irradiation potential (kWh/m^2/day)			
	Mean	Min	Max	Std
January	3.72	2.65	4.19	0.23
February	4.72	3.77	5.25	0.21
March	5.76	4.84	6.23	0.25
April	6.76	5.51	7.29	0.32
May	7.36	5.55	7.92	0.45
June	7.25	5.08	7.87	0.56
July	6.98	4.93	7.77	0.58
August	6.40	4.50	7.14	0.53
September	5.78	4.27	6.27	0.38
October	4.71	3.85	5.32	0.22
November	3.95	3.02	4.63	0.21
December	3.24	2.04	3.79	0.23

Regarding the Souss-Massa area, the minimum intensity is 3.33 kWh/m^2/day obtained in December versus 7.57 kWh/m^2/day as the maximum obtained in May. Furthermore, by comparing the annual average solar irradiation, it is apparent that Souss-Massa area study sites are more promising than the other European sites. Therefore, the south of Morocco in general and the Souss-Massa area in particular are blessed with an enormous solar potential for the deployment of solar PV projects and present an attractive option for potential investors.

4. Conclusion

Solar power systems represent an attractive option for clean energy production in the developing countries. Morocco has an enormous solar energy potential, especially in its southern regions. This study deals with the development of a model based on the MLP neural network technique to study the nonlinear function between the solar radiation and the geographical and meteorological parameters of the Souss-Massa region.

In this paper, we demonstrated the ability of ANN to accurately estimate the solar irradiation. Although the physical models based on satellite observations [57] provide accurate estimates of irradiation, they require testing and validation using data from ground meteorological stations [58]. This study proposes a method suitable for estimating the solar irradiation in zones where data from ground meteorological stations are unavailable as it is the

Table 4: Some of the largest photovoltaic power plants in Germany and Spain.

Country	Germany			Spain		
City	Strasskirchen	Köthen	Leipzig	Olmedilla	Puertollano	Arnedo
Nominal power (MWp)	54	45	40	60	47.5	34

Table 5: The monthly global solar irradiation comparison between the studied area and other European sites located in Germany and Spain.

	Monthly global solar irradiation in kWh/m^2/day								
Country	Germany			Spain			Souss-Massa region		
City	Strasskirchen	Köthen	Leipzig	Olmedilla	Puertollano	Arnedo	Agadir	Tata	Taroudant
January	0.79	0.64	0.67	2.14	2.23	1.85	3.75	4.02	3.74
February	1.54	1.31	1.32	3.18	3.33	2.65	4.8	4.98	4.73
March	3.09	2.69	2.69	4.65	4.73	4.15	5.96	5.98	5.64
April	4.58	4.26	4.26	5.51	5.57	4.92	6.93	7.03	6.78
May	5.25	5.18	5.18	6.64	6.67	5.8	7.56	7.69	7.46
June	5.7	5.65	5.59	7.64	7.74	6.75	7.27	7.64	7.54
July	5.4	5.22	5.24	7.98	8.06	7.18	7.04	7.22	7.4
August	4.6	4.37	4.41	6.85	7.04	6.17	6.49	6.59	6.78
September	3.3	3.17	3.14	5.28	5.26	4.78	5.94	6	6.01
October	2.0	1.9	1.89	3.81	3.9	3.24	4.78	4.99	4.71
November	1	0.83	0.84	2.45	2.58	2	4.05	4.21	3.9
December	0.6	0.53	0.54	1.96	2.06	1.65	3.27	3.57	3.15
Year	3.18	2.99	2.99	4.85	4.94	4.27	5.65	5.83	5.65

case in many African regions. In our work, we designed the ANN best model by using a selection of 24 site representatives of the different climates of the region. Then, the designed ANN is used in estimating the solar irradiation in the remaining 151 sites.

Generally, the results showed a good agreement between the measured and the estimated values. The analysis of solar maps, where irradiation is displayed using a color gradient from low to high intensity, showed that the southern-eastern and some inland sites seem more promising than other locations during most of the months; thus, they are more appropriate for solar technology. Also, these locations have an important solar potential during the year. Concerning the behavior of our model in mountainous locations, unstable results were obtained. This particular case reveals that the model was not fully able to estimate the solar irradiation because of a sudden change of temperature in some mountainous places.

Our developed model is highly valuable in providing the necessary irradiation data for designing and evaluating the performance of solar systems and can be exploited by engineers and researchers to inform renewable energy investors and decision makers about the appropriate planning and design of new solar plants. Also, this model is capable of generating valuable information about the solar potential in locations where there is a shortage of measurements, which will facilitate the selection task of high solar energy potential and the comparison between the best suitable sites.

To further advance this investigation, future research should focus on improving the procedure for selecting promising sites for the deployment of various solar energy technologies. Also, developing optimal ANN configurations which include the economic and environmental criteria in the selection task will be highly valuable.

Nomenclature

G_s: Measured global solar irradiation (kWh/m^2/day)
$\hat{G}_s$: Estimated global solar irradiation (kWh/m^2/day)
$\overline{G}$: Mean measured global solar irradiation (kWh/m^2/day)
R: Correlation coefficient
H: Number of hidden neurons
N: Number of input variables (neurons)
φ: Linear activation function at the output layer
$W_1(i,j)$: Weight between ith hidden layer neuron and jth input
$W_2(i)$: Weight between the output neuron and ith hidden layer neuron
X: Input parameter
X_j: jth element of the input parameter
H_i: Response of the ith hidden neuron
b_2: Bias value applied to the output layer neuron
$b_1(i)$: Bias value applied to the ith hidden layer neuron.

Acronyms

ANNs: Artificial neural networks

MLP: Multilayer perceptrons
LM: Levenberg-Marquardt
BP: Back propagation
MSE: Mean square error
MAE: Absolute mean error
RMSE: Root mean square error
rRMSE: Relative root mean square error.

Subscript

i: Neuron number of the hidden layer
j: Neuron number in the output layer.

Conflicts of Interest

The authors declare that they have no conflicts of interest.

Acknowledgments

This study was financed by IRSEN in the framework of Innotherm1-CSP Ait Baha project. The Moroccan Ministry of Higher Education and Research supported this study in the framework of the PPR 2015/31 project: Development of Solar Furnace with Heat Storage. The authors thank Rachid Ridouani who provided assistance with ArcGIS software during this study.

References

[1] R. Maurice, *Les énergies: Comparaisons techniques et socio-économiques*, LAVOISIER S.A.S, Paris, 2009th edition, 2009.

[2] J. R. Norris and M. Wild, "Trends in aerosol radiative effects over China and Japan inferred from observed cloud cover, solar "dimming," and solar "brightening"," *Journal of Geophysical Research Atmospheres*, vol. 114, no. 11, pp. 1–11, 2009.

[3] M. Wild, "Global dimming and brightening: a review," *Journal of Geophysical Research*, vol. 114, article D00D16, 2009.

[4] A. Assi, M. Al Shamisi, and M. Jama, "Prediction of monthly average daily global solar radiation in Al Ain City, UAE, using artificial neural networks," in *Proceedings of the 4th International Conference on Renewable Energy Sources (RES '10)*, pp. 109–113, Sousse, Tunisia, May 2010.

[5] W. Van Breusegem and S. Belhaj Mohamed, *Benefit Assessment Report for Morocco: 'Analysis for European Neighbourhood Policy (ENP) Countries and the Russian Federation on Social and Economic Benefits of Enhanced Environmental Protection'*, Morocco, 2011.

[6] S. Atouk, *Les énergies renouvelables et les populations rurales pauvres: le cas du Maroc*, Sherherooke University Canda, 2013.

[7] A. Amara, "Opening speech IRSEC 14, Ministry of Energy, Mines, Water and Environment," *Ministry of Energy, Mines, Water and Environment*, p. 5, 2014.

[8] B. E. Psiloglou and H. D. Kambezidis, "Performance of the meteorological radiation model during the solar eclipse of 29 March 2006," *Atmospheric Chemistry and Physics Discussions*, vol. 7, no. 4, pp. 12807–12843, 2007.

[9] B. P. Rand and J. Genoe, "Solar cells utilizing small molecular weight organic semiconductors," *Progress in Photovoltaics: Research and Applications*, vol. 15, pp. 659–676, 2007.

[10] F. Wang, Z. Zhen, Z. Mi, H. Sun, S. Su, and G. Yang, "Solar irradiance feature extraction and support vector machines based weather status pattern recognition model for short-term photovoltaic power forecasting," *Energy and Buildings*, vol. 86, pp. 427–438, 2015.

[11] H. D. Kambezidis and B. E. Psiloglou, "Recent improvements of the meteorological radiation model for solar irradiance estimates under all-sky conditions," *Renewable Energy*, vol. 93, pp. 142–158, 2016.

[12] A. Linares-rodriguez and J. A. Ruiz-arias, "An artificial neural network ensemble model for estimating global solar radiation from Meteosat satellite images," *Energy*, vol. 61, pp. 636–645, 2013.

[13] G. Zhang and B. E. Patuwo, "Forecasting with artificial neural networks: the state of the art," *International Journal of Forecasting*, vol. 14, pp. 35–62, 1998.

[14] V. Lo Brano, G. Ciulla, and M. Di Falco, "Artificial neural networks to predict the power output of a PV panel," *International Journal of Photoenergy*, vol. 2014, Article ID 193083, 12 pages, 2014.

[15] D. Fadare and I. Irimisose, "Modeling of solar energy potential in Africa using an artificial neural network," *American Journal of Scientific and Industrial Research*, vol. 1, no. 2, pp. 144–157, 2010.

[16] K. S. Reddy and M. Ranjan, "Solar resource estimation using artificial neural networks and comparison with other correlation models," *Energy Conversion and Management*, vol. 44, no. 15, pp. 2519–2530, 2003.

[17] J. T. Lin and D. Bhattacharyya, "Multiple regression and neural networks analyses in composites machining," *Composites Science and Technology*, vol. 63, no. 3-4, pp. 539–548, 2003.

[18] G. Landeras, J. J. López, O. Kisi, and J. Shiri, "Comparison of gene expression programming with neuro-fuzzy and neural network computing techniques in estimating daily incoming solar radiation in the Basque Country (Northern Spain)," *Energy Conversion and Management*, vol. 62, pp. 1–13, 2012.

[19] J. Waewsak and C. Chancham, "Estimation of monthly mean daily global solar radiation over Bangkok, Thailand using artificial neural networks," *Energy Procedia*, vol. 57, pp. 1160–1168, 2014.

[20] O. Şenkal, "Modeling of solar radiation using remote sensing and artificial neural network in Turkey," *Energy*, vol. 35, no. 12, pp. 4795–4801, 2010.

[21] T. Khatib, A. Mohamed, K. Sopian, and M. Mahmoud, "Solar energy prediction for Malaysia using artificial neural networks," *International Journal of Photoenergy*, vol. 2012, Article ID 419504, 16 pages, 2012.

[22] A. Mellit and A. M. Pavan, "A 24-h forecast of solar irradiance using artificial neural network: application for performance prediction of a grid-connected PV plant at Trieste, Italy," *Solar Energy*, vol. 84, no. 5, pp. 807–821, 2010.

[23] D. A. Fadare, "Modelling of solar energy potential in Nigeria using an artificial neural network model," *Applied Energy*, vol. 86, no. 9, pp. 1410–1422, 2009.

[24] J. C. Lam, K. K. W. Wan, and L. Yang, "Solar radiation modelling using ANNs for different climates in China," *Energy Conversion and Management*, vol. 49, no. 5, pp. 1080–1090, 2008.

[25] A. Ouammi and D. Zejli, "Artificial neural network analysis of Moroccan solar potential," *Renewable and Sustainable Energy Reviews*, vol. 16, pp. 4876–4889, 2011.

[26] J. Terrapon-Pfaff and S. Borbonus, *Energy and Development: Exploring the Local Livelihood Dimension of the Nooro I CSP Project in Southern Morocco*, Germany, 2015.

[27] the free encyclopedia Wikipedia, "Souss-Massa area, Wikipedia, the free encyclopedia," 2015, August 2016, https://fr.wikipedia.org/wiki/Souss-Massa.

[28] Souss Massa Regional Directorate, "Presentation of the Souss Massa region, Haut-commissariat au plan," 2015, August 2016, http://www.hcp.ma/region-agadir/Presentation-de-la-region-de-Souss-Massa_a16.html.

[29] K. Saravanan and S. Sasithra, "Review on classification based on artificial neural networks," *The International Journal of Ambient Systems and Applications*, vol. 2, no. 4, pp. 11–18, 2014.

[30] W. Yao-wu and D. R. Aryal, "Neural network forecasting of the production level of Chinese construction industry," *Journal of Comparative International Management*, vol. 6, no. 2, pp. 45–64, 2003.

[31] F. Azam, *Biologically Inspired Modular Neural Networks*, the Faculty of the Virginia Polytechnic Institute, 2000.

[32] D. P. Kanungo and M. K. Arora, "A comparative study of conventional, ANN black box, fuzzy and combined neural and fuzzy weighting procedures for landslide susceptibility zonation in Darjeeling Himalayas," *Engineering Geology*, vol. 85, no. 3-4, pp. 347–366, 2006.

[33] S. A. Kalogirou, "Artificial neural networks in renewable energy systems applications: a review," *Renewable and Sustainable Energy Reviews*, vol. 5, no. 4, pp. 373–401, 2001.

[34] J. Mao and K. M. Mohluddin, "Why artificial neural networks," *IEEE*, vol. 29, pp. 31–44, 1996.

[35] M. S. Aït Cheikh, M. Haddadi, and A. Zerguerras, "For the maximum power point tracking (MPPT)," *Revue des Energies Renouvelables*, vol. 10, pp. 109–118, 2007.

[36] I. Yilmaz and O. Kaynar, "Multiple regression, ANN (RBF, MLP) and ANFIS models for prediction of swell potential of clayey soils," *Expert Systems with Applications*, vol. 38, no. 5, pp. 5958–5966, 2011.

[37] C. M. Bishop, *Neural Network for Pattern Recognition, 2013 Repr*, Oxford University Press, Oxford, 1995.

[38] P. W. Stackhouse, W. S. Chandler, T. Zhang, D. Westberg, A. J. Barnett, and J. M. Hoell, "Surface meteorology and solar energy (SSE) release 6.0 methodology version 3.2.0," *NASA*, p. 76, 2016.

[39] W. Paul, "Stackhouse and site administration/help: NASA Langley ASDC user services," *Surface Meteorology and Solar Energy NASA*2017, June 2017, https://eosweb.larc.nasa.gov/cgi-bin/sse/sse.cgi?skip@larc.nasa.gov+s01+s05+s06+s07+s09+s10#s06.

[40] A. Ohmura, H. Gilgen, and H. Hegner, "Baseline surface radiation network (BSRN/WCRP): new precision radiometry for climate research," *Bulletin of the American Meteorological Society*, vol. 79, no. 10, pp. 2115–2136, 1998.

[41] M. Rumbayan, A. Abudureyimu, and K. Nagasaka, "Mapping of solar energy potential in Indonesia using artificial neural network and geographical information system," *Renewable and Sustainable Energy Reviews*, vol. 16, no. 3, pp. 1437–1449, 2012.

[42] Neural Network Toolbox, "Improve neural network generalization and avoid overfitting, the MathWorks, Inc.," 2016, May 2016, http://www.mathworks.com/help/nnet/ug/improve-neural-network-generalization-and-avoid-overfitting.html#bt0cnqi.

[43] G. López and F. Batlles, "Selection of input parameters to model direct solar irradiance by using artificial neural networks," *Energy*, vol. 30, no. 9, pp. 1675–1684, 2005.

[44] A. Koca and H. F. Oztop, "Estimation of solar radiation using artificial neural networks with different input parameters for Mediterranean region of Anatolia in Turkey," *Expert Systems with Applications*, vol. 38, no. 7, pp. 8756–8762, 2011.

[45] S. Rehman and M. Mohandes, "Artificial neural network estimation of global solar radiation using air temperature and relative humidity," *Energy Policy*, vol. 36, no. 2, pp. 571–576, 2008.

[46] V. Badescu, *Modeling Solar Radiation at the Earth's Surface*, Springer, Romania, 2008.

[47] G. Ciulla, V. Lo Brano, and E. Moreci, "Forecasting the cell temperature of PV modules with an adaptive system," *International Journal of Photoenergy*, vol. 2013, Article ID 192854, 10 pages, 2013.

[48] L. Prechelt, *Neural Networks: Tricks of the Trade, Vol. 7700*, Springer Berlin Heidelberg, Berlin, Heidelberg, 2012.

[49] M. H. Beale and M. T. Hagan, *Neural Network Toolbox™ User's Guide*, The MathWorks; Inc., 3 Apple Hill Drive Natick; MA 01760–2098, 2015.

[50] M. T. Hagan and M. B. Menhaj, "Training feedforward networks with the Marquardt algorithm," *IEEE Transactions on Neural Networks*, vol. 5, no. 6, pp. 989–993, 1994.

[51] A. Bulsari and H. Saxen, "Application of artificial neural networks for filtering, smoothing and prediction for a biochemical process," *Expert Systems*, vol. 11, no. 3, pp. 159–166, 1994.

[52] B. G. Kermani and S. S. Schiffman, "Performance of the Levenberg–Marquardt neural network training method in electronic nose applications," *Sensors and Actuators B: Chemical*, vol. 110, no. 1, pp. 13–22, 2005.

[53] T. Khatib, A. Mohamed, K. Sopian, and M. Mahmoud, "Assessment of artificial neural networks for hourly solar radiation prediction," *International Journal of Photoenergy*, vol. 2012, Article ID 946890, 7 pages, 2012.

[54] M. A. De Oliveira and O. Possamai, "Modeling the leadership - project performance relation: radial basis function, Gaussian and Kriging methods as alternatives to linear regression," *Expert Systems with Applications*, vol. 40, no. 1, pp. 272–280, 2013.

[55] S. P. P. I. Center, "Solar power plants information center, list of photovoltaic power plants in the world," 2009, September 2016, http://solarenergypowerplants.blogspot.com/search?q=olmedilla.

[56] H. Thomas and D. Ewan, "JRC's Institute for Energy and Transport-PVGIS-European Commission," 2012, September 2016, http://re.jrc.ec.europa.eu/pvgis/about_pvgis/about_pvgis.htm.

[57] I. F. Trigo, C. C. Dacamara, F. Viterbo et al., "The satellite application facility for land surface analysis," *International Journal of Remote Sensing*, vol. 32, no. 10, pp. 2725–2744, 2011.

[58] J. Polo, L. F. Zarzalejo, M. Cony et al., "Solar radiation estimations over India using Meteosat satellite images," *Solar Energy*, vol. 85, no. 9, pp. 2395–2406, 2011.